Journal of Multidisciplinary Engineering Science and Technology (JMEST)
ISSN: 2458-9403
Vol. 7 Issue 4, April - 2020

Achieving Robustness of a Renewable Energy Light Tracker Control System

Prof. Kamen M. Yanev
Department of Electrical and Electronic Engineering
New Era College of Arts, Science and Technology
Gaborone, Botswana
yanevkm@yahoo.com; kyanev@neweracollege.ac.bw

***Abstract*—Fixed photovoltaic (PV) modules are able to convert only a fraction of the light energy from the sun into electric energy. A tracking system constantly adapts the angle of PV modules so that the irradiation angle and the light intensity remain constant and a maximum of electrical energy can be generated. This not only helps to exploit every minute of sunshine but also to make the best use of diffuse light all year round. Due to the changes of the conditions of operation, a tracking PV system shows signs of variation of its parameters. The aim of this research is to analyze the stability of a typical single axes PV system, affected by its parameter variations and improve its performance and robustness. This is achieved by the design of a specialized robust controller and the application of the method of the Advanced D-partitioning.**

Keywords—solar, photovoltic tracking system, robust control, Advanced D-partitioning

I. INTRODUCTION

For flat-panel photovoltaic systems, trackers are used to minimize the angle between the incoming sunlight and a photovoltaic panel. Depending on the type of tracking system, the panel is either aimed directly at the sun or the brightest area of a partly clouded sky. A control unit detects the spot in the sky with the most intense light and adjusts the PV module surface position to face it. A solar panel in a fixed orientation between the dawn and sunset extremes will see a motion of 75 degrees to either side and therefore will lose over 75% of the energy in the morning and evening [1]. Rotating the panels to the east and west can help recapture those losses. A tracker that only attempts to compensate for the east-west movement of the sun is known as a single-axis tracker. Even on a completely cloudy day, the module surface is adjusted to face the point of the strongest irradiation. If a day starts off sunny with clouds moving from the west in the afternoon, the module surface will then move back slightly towards the east.

A tracker that accounts for both the daily and seasonal motions is known as a dual-axis tracker. Generally speaking, the losses due to seasonal angle changes are complicated by changes in the length of the day, increasing collection in the summer in northern or southern latitudes. There is considerable argument within the industry whether the small difference in yearly collection between single and dual-axis trackers makes the added complexity of a two-axis tracker worthwhile. A recent review of actual production statistics suggested the difference was about 4% in total, which was far less than the added costs of the dual-axis systems [2], [3]. This compares unfavourably with the 24-32% improvement between a fixed-array and single-axis tracker.

On daily basis changes in the ambient temperature may cause variation of some of the parameters of the photovoltaic systems [4]. In general, the gain of the tracking system is sensitive to temperature variation and this may initiate system vibrations due to oscillations in the system response. All other system parameters are considered approximately constant.

Control systems must have performance that is robust or insensitive to parameter variations. In the process of design of a robust control system, it is important to determine the regions of stability, corresponding to the variation of a specific system parameter [5]. The system will be analyzed with the method of the Advanced D-partitioning that was suggested by the author in 2005 [6], [7]. The method will explore the effects of the gain variations on system's stability. The method employs the possibility to define regions of stability in the space of the system's parameters.

One of the contributions of this research is to simplify and graphically determine the regions of stability for variation of a specific system parameter. Further to this analysis, the paper contributes in suggesting a strategy of design of a robust control system by introducing a robust controller that enforces a desired system performance.

II. STRUCTURE AND ANALYSIS OF A SINGLE-AXIS TRACKING PV SYSTEM

A Comparison between a PV fixed and PV single-axis tracking system is demonstrated in Figure 1. It is seen that while a PV fixed tilted system delivers its maximum output power in the rate of 1Mw/m^2 only at around 1:12 PM, a single-axes PV tracking system delivers maximum output power close to 1Mw/m^2 during the time interval from 9:00 AM to 6:00 PM.

It is obvious that the PV single-axis tracking system utilizes significant power in the early mornings and late afternoons while the fixed PV solar panel system becomes unable to collect a reasonable proportion of the available energy [4], [7].

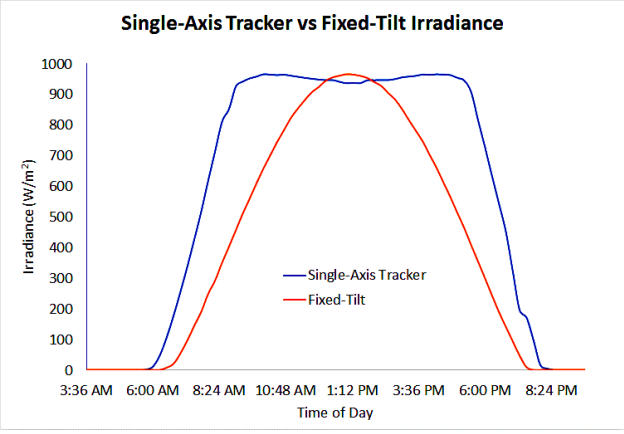

Figure 1: Comparison between Fixed-tilt PV Systems and Single – Axes PV Tracker Systems Efficiency

As seen from Figure 2, the PV panels of the single-axes PV tracking system are also tilted up to proper degrees, necessary to maintain the best angle that is south or north toward the sun. The maximum annual energy production is achieved when the array is tilted at the specific latitude angle of the system location.

Figure 2: Single–Axes PV Tracker System aiming at the Brightest Point in the Sky

The tracking platforms can rotate the surface of the PV arrays along an axis with the help of a motor. The motor itself is connected to a control system that determines the position of the sun. Trackers can be passive or active. Passive systems tend to be moving slowly from the sunrise to the sunset position. Active trackers use light sensors that will point the PV modules to the brightest point in the sky, not necessarily the sun, especially when it is cloudy [5].

The typical operation of a single-axes PV active tracking system [6], [7] can be described from the diagram shown in Figure 3.

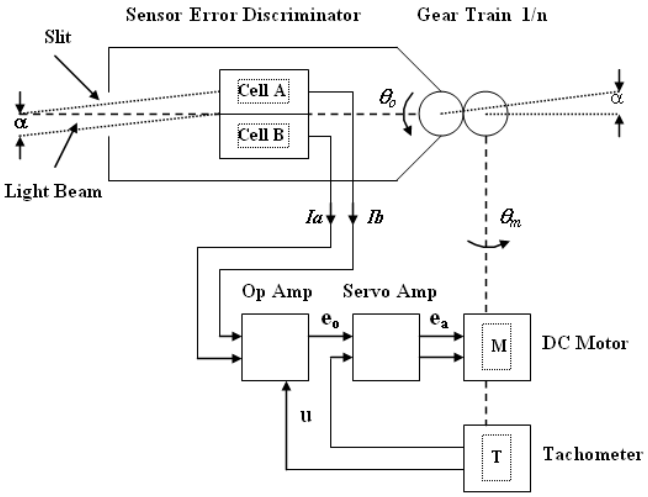

Figure 3: Single-Axes PV Active Tracking System

The tracking sensor is an error discriminator, consisting of two photovoltaic cells mounted behind a rectangular slit in a cylinder enclosure. The cells are mounted in such a way that when the sensor is pointed at the brightest point in the sky, a beam of light from the slit overlaps both cells.

The sensor itself is mounted at 90° to the surface of the PV panels. The photovoltaic cells are used as current sources and are connected in opposite polarity to the input of an operational amplifier. Any difference in the currents of the two sells is sensed and amplified by the operational amplifier.

Since the current of each cell is proportional to the illumination on the cell, an error signal will be present at the output of the amplifier when the light from the slit is not precisely aligned on the cells. This error voltage when fed to the servo-amplifier will cause the motor to drive the system back into alignment.

The block diagram of the light tracking system is shown in Figure 4. The input variable θ_r represents the reference angle of the bright light beam, while θ_o matches the sensor axis. The difference between these two angles depicts the error α. The objective of the light tracking system is to maintain the error α between θ_r and θ_o near zero. The parameters of the system are chosen as follows: Sensor constant K_s = 0.01 A/rad; OP constant R_F = 1000; **Servo amplifier gain K = Variable**; DC motor gain constant K_i = 0.0125 Nm/A; Armature resistance R_a = 6.25Ω; Armature inductance L_a = 0.01H; Inertia J = 10^{-6} kg.m^2; Damping B = 0; Motor constant K_b = 0.0125V/rad/sec; Motor speed n = 800.

Initially, the transfer function of the robust controller is assumed to be $G_C(s)$ = 1. Taking into account the system identification [5] and mathematical

description of its components, the transfer function of the DC motor can be represented as:

$$\frac{\theta_m}{e_a} = \frac{K_i}{JL_a s^3 + (R_a J + L_a B)s^2 + (R_a B + K_b K_i)s} \quad (1)$$

Considering the mathematical description of all the single-axes PV active tracking system components [8], [9] and substituting the system parameters values, the transfer function of the complete open-loop system is presented as follows:

$$G_{OL} = \frac{K_S R_F K K_i / n}{JL_a s^3 + (R_a J + L_a B)s^2 + (R_a B + K_b K_i)s} = \quad (2)$$
$$= \frac{K}{s(1+0.02s)(1+0.005s)}$$

Then the transfer function of the complete closed-loop system is presented as follows:

$$G_P(s) = \frac{K}{s(1+0.02s)(1+0.005s)+K} \quad (3)$$

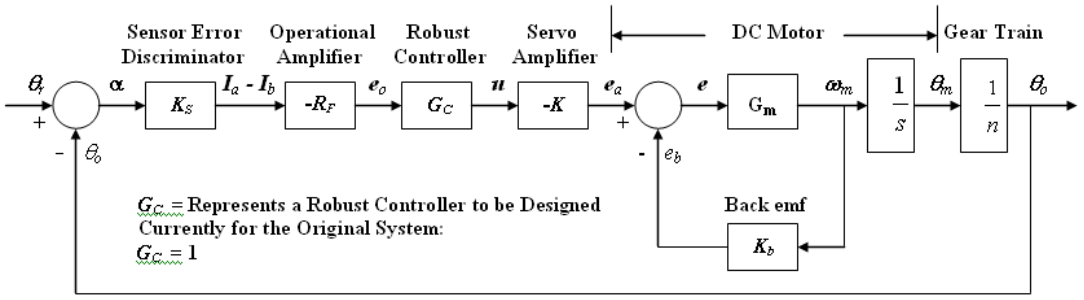

Figure 4: Block Diagram of the Single-Axes PV Active Light Tracking System

The characteristic equation of the closed-loop system is determined as:

$$G(s) = s(1+0.02s)(1+0.005s) + K = 0 \quad (4)$$

The servo amplifier gain *K* is the variable system's parameter and can be determined by applying the method of the Advanced D-partitioning [6], [10].

The gain *K* can be obtained from the system's characteristic equation as follows:

$$G(s) = P(s) + KQ(s) = 0 \quad (5)$$

Where

$$P(s) = s(1+0.02s)(1+0.005s) \quad (6)$$

$$Q(s) = 1 \quad (7)$$

$$K(s) = -\frac{P(j\omega)}{Q(j\omega)} = -\frac{0.0001s^3 + 0.025s^2 + s}{1} \quad (8)$$

The D-partitioning curve of the variable gain *K*, is obtained by substituting $s = j\omega$ in (6) and varying the frequency within the range $-\infty \le \omega \le +\infty$ [6], [7], [10]. Following the proposed MATLAB procedure, the corresponding D-partitioning curve in terms of the variable parameter *K* is shown in Figure 5:

```
>> Gp = tf([1],[0.0001 0.025 1 0])
>> [den,num]=tfdata(-A1,'v')
den =  0    0    0   -1
num = 0.0001  0.0250  1.0000   0
>> K=tf(num,den)
>> dpartiton(K)
```

The D-partitioning regions are obtained graphically in the *K*-plane by allocating values of the frequency within the range $-\infty \le \omega \le +\infty$.

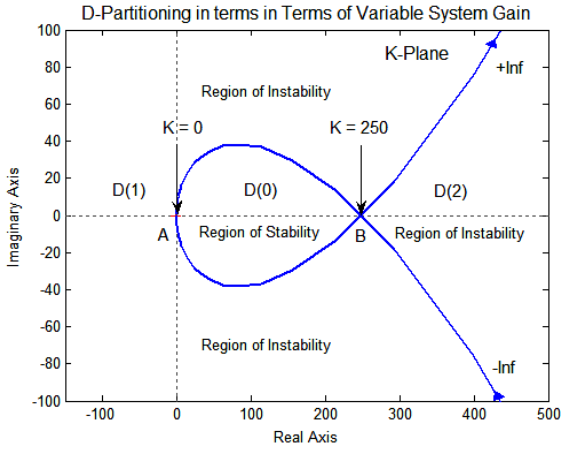

Figure 5: Advanced D-Partitioning Analysis in Terms of the Variable Servo Amplifier Gain K

The D-partitioning shown in Figure 5 determines three regions on the *K*-plane: D(0), D(1) and D(2). According to the method of the Advanced D-Partitioning, only D(0) is the region of stability, since it is the one, being always on the left-hand side of the D-partitioning curve for a frequency variation from $-\infty$ to $+\infty$ [7], [8], [10]. The system is stable within the gain range $0 \le K \le 250$ corresponding to the segment *AB*, being within the stable region. At point *B*(250, j0) the gain is *K* = 250 and the system becomes marginal.

The D-partitioning curve in terms of one variable parameter can be plotted in the complex plane within the frequency range $-\infty \le \omega \le +\infty$, facilitated by MATLAB the "nyquist" m-code. To avoid any misinterpretation of the Advanced D-Partitioning procedure, the "nyquist" m-code is modified into a

"dpartition" m-code with the aid of the MATLAB Editor and a proper formatting. The "dpartition" m-code will plot the curve of a specific system parameter in terms of the frequency variation from $-\infty$ to $+\infty$ exactly similar to the "nyquist" m-code, but it can work only on a computer where the new developed "dpartition" m-code is included in the MATLAB program [11].

In order to benefit from the Advanced D-Partitioning analysis shown in this research, the wider engineering community can still use the "nyquist" m-code for the purpose of plotting the D-partitioning curve. The "nyquist" m-code will actually also plot the curve of $K(j\omega)$ within the frequency range $-\infty \le \omega \le +\infty$.

The results obtained from the analysis with the aid of the Advanced D-partitioning can be compared with the outcome from the system's assessment with the aid of the Bode stability criterion [11], [12]. There is a close relationship between the results from the Advanced D-partitioning and the Bode stability criterion analysis. The system open-loop transfer function at servo amplifier gain K = 250 is presented at equation (9). Achieved by the code below and shown in Figure 6, the Bode diagrams of the open-loop system confirm that the control system is marginal when the system's gain reaches its critical value K = 250. At this state the system's Gain Margin (G.M. =0) and the Phase Margin (P.M. = 0).

$$G_{OL}(s) = \frac{250}{0.0001s^3 + 0.025s^2 + s} \tag{9}$$

```
>> GoL = tf([250],[0.0001 0.025 1 0])

Transfer function:
        250
-------------------------
0.0001 s^3 + 0.025 s^2 + s

>> bode(GoL)
```

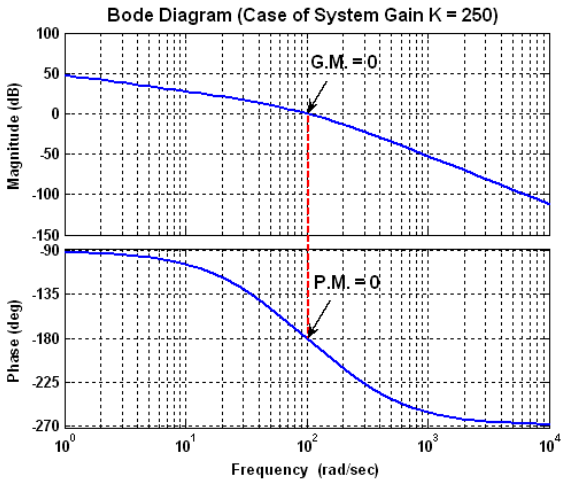

Figure 6: Confirmation of the Marginal Gain of Stability with the Aid of the Bode Stability Criterion [GM = 0, PM = 0]

The Advanced D-partitioning results can be compared also with the outcome the application of the Nyquist stability criterion [11], [12]. Again, there is a close relationship between the results of the two different analysis methods.

Achieved by the code shown below and presented in Figure 7, the Nyquist diagram of the open-loop system crosses the negative part of the real axes exactly at a point (-1, j0). This confirms the marginal state of the control system when the servo amplifier gain is at its critical value K = 250.

```
>> GoL = tf([250],[0.0001 0.025 1 0])

Transfer function:
        250
-------------------------
0.0001 s^3 + 0.025 s^2 + s

>> nyquist(GoL)
```

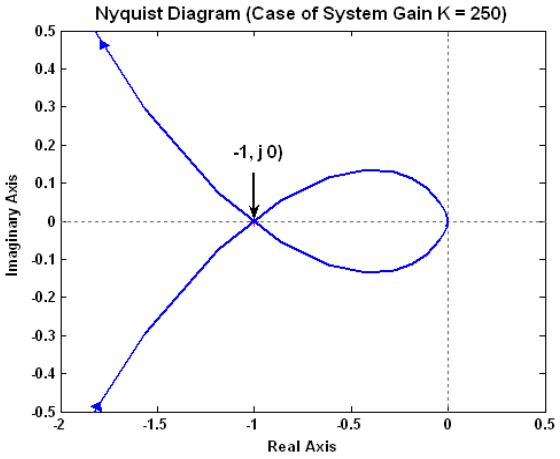

Figure 7: Confirmation of the Marginal Gain of Stability with the Aid of the Nyquist Stability Criterion (-1, j0)

The step response of the system is examined for robustness, considering a number of gain values within the gain range $0 \le K \le 250$ and the results are shown in Fig. 7.

It is seen that the step response of the closed-loop system varies considerably for different values of the gain K while its steady-state error is $e_{ss} = 0$.

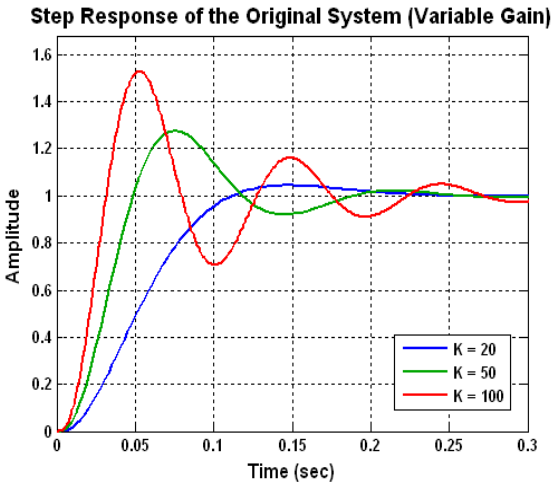

Figure 8: Responses of the System with a Variable Gain

Higher values of the servo amplifier gain K may cause considerable oscillation, instability and destruction of the control system.

III. Design of a Robust Controller and Achieving the Best PV System's Performance

A control system is robust when maintains certain properties like stability and performance in spite of external disturbances, noise or parameter variations.

The "Integral of Time multiplied by the Absolute value of Error" (ITAE) [6], [8], [14] reaches a minimum value for a relative damping ratio ζ = 0.707. One of the solutions to meet the ITAE criterion is to implement a robust controller consisting of a series and a forward stage. The controller design employs a two-step zero-pole cancelation [9], [14] that enforces a desired system damping, stability and time response.

The design strategy for constructing the series stage of the controller is to place its two zeros near the desired closed-loop poles, that satisfy the condition ζ = 0.707.

The closed-loop transfer function shown in equation (1) can be also presented as follows:

$$G_{PK}(s) = \frac{10000\,K}{s^3 + 250s^2 + 10000\,s + 10000\,K} \tag{10}$$

By applying the ITAE criterion, the optimal value of the closed-loop system gain *K,* corresponding to the damping ratio ζ = 0,707, is determined from the following MATLAB procedure and is presented graphically in Figure 8:

```
K=[15:0.01:25];
>> for n=1:length(K)
G_array(:,:,n)=tf([10000*K(n)],[1 250 10000 10000*K(n)]);
   end
>> [y,z]=damp(G_array);
>> plot(K,z(1,:))
```

The relationship between the Damping Ratio ζ and the gain *K* is presented graphically in Figure 9:

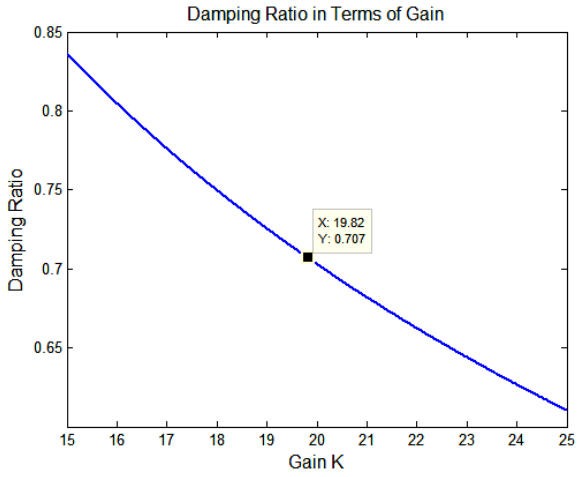

Figure 9: Optimal Gain Value Corresponding to Damping Ratio ζ=0,707

As shown from Fig. 9, if the system's gain is tuned to *K* = 19.82, the relative damping ratio becomes ζ = 0.707. Then the transfer function of the closed-loop system is modified to:

$$G_P = \frac{198200}{s^3 + 250s^2 + 10000\,s + 198200} \tag{11}$$

This condition corresponds to the desired closed-loop poles –21.9 ± j21.9, which are determined as follows:

```
>> GP=tf([198200],[1 250 10000 198000])
   Transfer function:
   198200
   -------------------------------
   s^3 + 250 s^2 + 10000 s + 198000
>> pole(GP)
   ans =
   1.0e+002 *
   -2.0615
   -0.2192 + 0.2190i
   -0.2192 - 0.2190i
>> damp(GP)
Eigenvalue              Damping     Freq. (rad/s)
-2.19e+001 + 2.19e+001i 7.07e-001   3.10e+001
-2.19e+001 - 2.19e+001i 7.07e-001   3.10e+001
-2.06e+002              1.00e+000   2.06e+002
```

The two zeros of the series controller stage can be placed at –22 ± j22. Thus, the transfer function of the series robust controller $G_S(s)$ is presented as:

$$G_S(s) = \frac{(s + 22 + j22)(s + 22 - j22)}{9.68} = \frac{s^2 + 44s + 968}{968} \tag{12}$$

To realize physically the controller G_S (s), two controller poles, at –1250, j0, are added so that their effect on the system performance is negligible [6], [11].

However, to simplify the analysis, the transfer function of the open-loop system after applying the series controller will still be determined from the equations (3) and (12) as follows:

$$G_{OL}(s) = G_S(s)G_P(s) = \frac{0.001K(s^2 + 44s + 968)}{s(1 + 0.02s)(1 + 0.005s)} \tag{13}$$

The unity feedback closed-loop transfer function becomes:

$$G_{CL}(s) = \frac{0.001K(s^2 + 44s + 968)}{s(1 + 0.02s)(1 + 0.005s) + 0.1K(s^2 + 44s + 968)} \tag{14}$$

As seen from the equations (13) and (14), the zeros are in the close vicinity to the poles of the closed-loop transfer function and will cancel them. To avoid this problem, a forward controller G_F(s) [12] is added to the closed-loop system.

The poles of $G_F(s)$ should cancel the zeros of the closed-loop transfer function $G_{CL}(s)$. The transfer function of the forward controller is designed as:

$$G_F(s) = \frac{968}{s^2 + 44s + 968} \quad (15)$$

The complete control system, incorporating the two-stage robust controller is shown in Fig. 10.

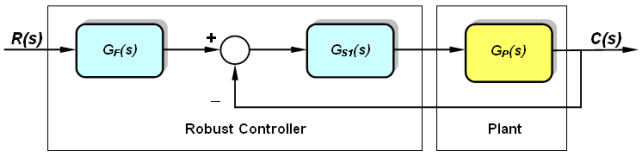

Figure 10: Robust Controller Incorporated in the System

From the block diagram in Figure 10, the transfer function of the total compensated control system is:

$$G_T(s) = G_F(s)G_{CL}(s) = \frac{K}{s(1+0.02s)(1+0.005s) + 0.001K(s^2 + 44s + 968)} \quad (16)$$

The D-partitioning in terms of the variable gain K can be determined from the characteristic equation based on the total system G_T (s) and following the procedure:

$$K = -\frac{0.0001s^3 + 0.025s^2 + s}{0.001s^2 + 0.044s + 2} \quad (17)$$

```
>> K = tf([-0.0001 -0.025 -1 0],[0.001 0.044 2])
>> dpartiton(K)
```

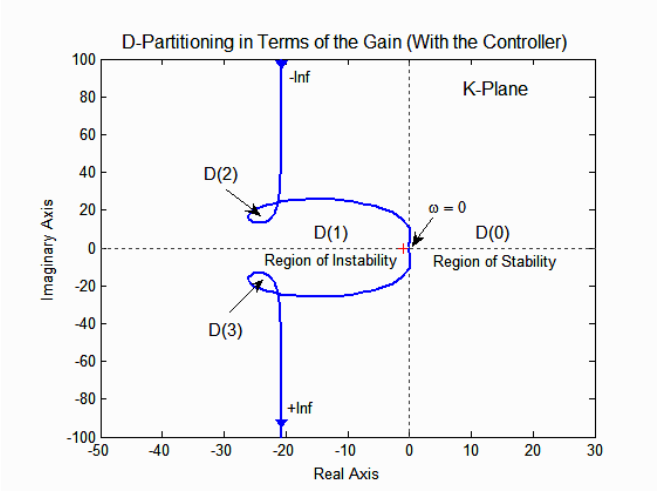

Figure 11: D-Partitioning Including the Robust Controller

As seen from Figure 11, the D-partitioning determines four regions of the K-plane: D(0), D(1), D(2) and D(3). Only D(0) is the region of stability, since it is located always on the left-hand side of the D-partitioning curve for a frequency variation from $-\infty$ to $+\infty$ [12], [13], [15]. From Figure 10, it is seen that the system will be stable for any values of $K > 0$, since any such value of the gain is located in D(0).

The compensated system is being examined for robustness in the time-domain, substituting a number of values for the gain K = 100, 200 and 500 in equation (16):

$$G_{T1}(s)_{K=100} = \frac{100}{s(1+0.02s)(1+0.005s) + 0.02(s^2 + 44s + 968)} = \frac{100}{0.0001s^3 + 0.045s^2 + 1.88s + 19.36} \quad (18)$$

$$G_{T2}(s)_{K=200} = \frac{200}{s(1+0.02s)(1+0.005s) + 0.05(s^2 + 44s + 968)} = \frac{200}{0.0001s^3 + 0.075s^2 + 3.2s + 48.4} \quad (19)$$

$$G_{T3}(s)_{K=500} = \frac{500}{s(1+0.02s)(1+0.005s) + 0.1(s^2 + 44s + 968)} = \frac{500}{0.0001s^3 + 0.125s^2 + 5.4s + 96.8} \quad (20)$$

Finally the step responses of the robust control system at different gain values are determined by the following procedure and are presented in Figure 12:

```
>> GT1 = tf([100],[0.0001 0.045 1.88 19.36])
>> GT2 = tf([200],[0.0001 0.075 3.2 48.4])
>> GT3 = tf([500],[0.0001 0.125 5.4 96.8])
>> step(GT1,GT2,GT3)
```

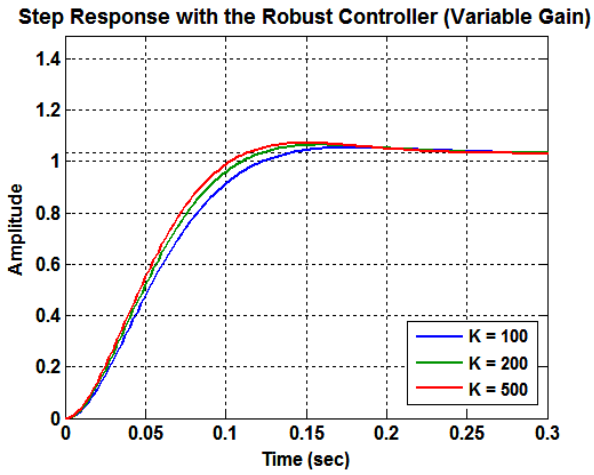

Figure 12: Step Responses of the Robust System for Gains (K = 100, 200, 500)

It is seen from Fig. 12 that due to the effect of the applied robust controller, the compensated system becomes quite insensitive to even larger variations of the system's gain K *(K = 100, 200* and *500)*.

If the values K = *20, 50* and *100* are applied, the step response curves are close coincide with each other. It is also observed that the robust controller introduces a negligible steady-state error $e_{ss} \neq 0$.

IV. CONCLUSION

The PV light tracking system may experience poor performance or become unstable due to variation of system's parameters. Specifically the system's gain is subjected to uncertainty due to ambient temperature variations.

The design strategy of the robust controller is based on the application of the ITAE criterion. A two-step zero-pole cancelation is introduced, enforcing a desired system damping, stability and time response.

The light tracking system is analyzed before and after the application of the robust controller with the aid of the method of the Advanced D-partitioning. This method for system stability analysis, suggested by the author in 2005, proves to be very efficient for graphical determination of the regions of stability in terms of system's uncertain or variable parameters.

The system robustness is examined after applying the robust controller and the obtained results demonstrate its insensitivity in terms of gain variations. The robust controller efficiency is also successfully tested for the cases of time constants variations or even for simultaneous variation of several different system parameters. As a result of its application the control system becomes insensitive to any parameter uncertainties within specific limits.

After applying the robust controller, the robust PV light tracking system has no oscillations and becomes insensitive to system's parameter changes. This proves to be of high importance for the system operation, since due to clouds or other atmospheric effects the direction of the brightest light may rapidly change.

With the robust controller, the system avoids stress and vibrations and is smoothly redirecting the PV panel to its new position.

REFERENCES

[1] A. Zaher, "Optimization of Solar Tracking Systems", International Journal of Energy and Power Engineering, Vol: 12, No:5, 2018, pp.367-371.

[2] PV Tracking Solar System, Retrieved March 23, 2018, from http://www.careyglasssolar.com/pv-tracking- system-solar-panel.php

[3] PV Tracking Applications, Retrieved March 24, 2018, from http://www.renewableenergyworld.com/rea/news/article/2009/03/pv-tracking-applications-gather-momentum

[4] Solar Tracker, Retrieved March 25, 2018,from http://en.wikipedia.org/wiki/Solar_tracker

[5] F. Golnaraghi, B. Kio, Automatic Control Systems, John Wiley & Sons, Inc, 9th Edition, ISBN 978-0-470-04896-2, 2014, p. 576-589.

[6] K.M. Yanev, "Application of the Method of the D-Partitioning for Stability of Control Systems with Variable Parameters", *Botswana Journal of Technology,* Vol. 15,N.1, 2005, pp.26-33.

[7] K.M. Yanev, "Analysis of Systems with Variable Parameters and Robust Control Design", *Sixth IASTED International Conference on Modeling, Simulation And Optimization,* 2006, pp. 75-83.

[8] M. H. Moulahi, F. Ben Hmida, M. Gossa, "Robust Fault Detection for Stochastic Linear Systems in Presence the Unknown Disturbance: Using Adaptive Thresholds", *International Review of Automatic Control (IREACO),* Napoli, Italy, Vol. 3, N.1, 2010, pp.11-23.

[9] K.M. Yanev, "Design and Analysis of a Robust Accurate Speed Control System by Applying a Digital Compensator", *ICGST, Journal of Automatic Control and System Engineering*, Delaware, USA, Volume 16, Issue 1, ISSN: 1687-4811,2016, pp.27-36.

10] K.M. Yanev, G.O. Anderson, S. Masupe, "Strategy for Analysis and Design of Digital Robust Control Systems", *ICGST, Journal of Automatic Control and System Engineering*, Delaware, USA, Volume 12, Issue 1, ISSN: 1687-4811,2012, pp.37-44.

[11] K.M. Yanev, "Advanced D-Partitioning Stability Analysis of Digital Control Systems with Multivariable Parameters", *ICGST, Journal of Automatic Control and System Engineering*, Delaware, USA, Volume 16, Issue 1, ISSN: 1687-4811, 2016, pp. 9-19.

[12] K.M. Yanev, G.O. Anderson, ObokOpok, "Achieving Robustness in Control Systems with Variable Time-Constants", *International Journal of Energy Systems, Computers and Control,* Vol. 1, (Issue 1), 2011, pp.1-14.

[13] K.M. Yanev, S. Masupe, "Robust Design and Efficiency in Case of Parameters Uncertainties, Disturbances and Noise", International Review of Automatic Control, Italy, ISSN: 1974-6059, Vol. 5, N. 6

[14] S. Shinners,"Modern Control System Theory and Application", Addison Wesley Publishing Company, London, 2008, pp. 43-46.

[15] K.M. Yanev, "Analysis and Design of Servo Robust Control System", *International Review of Automatic Control (IREACO),* ISSN: 1974-6059, Vol. 7, N. 2, 2014, pp. 217-224.